J. Plasma Physics (2012), vol. 78, part 4, pp. 455–459. © Cambridge University Press 2012
doi:10.1017/S0022377812000335

Optimum angle for side injection of electrons into linear plasma wakefields

K. V. LOTOV

Budker Institute of Nuclear Physics SB RAS, Novosibirsk, 630090, Russia
Novosibirsk State University, Novosibirsk, 630090, Russia
(K.V.Lotov@inp.nsk.su)

(Received 28 September 2011; revised 12 December 2011; accepted 19 March 2012; first published online 12 April 2012)

Abstract. A unified model of electron penetration into linear plasma wakefields is formulated and studied. The optimum angle for side injection of electrons is found. At smaller angles, all electrons are reflected radially. At larger angles, electrons enter the wakefield with superfluous transverse momentum that is unfavorable for trapping. Separation of incident electrons into penetrated and reflected fractions occurs in the outer region of the wakefield at some 'reflection' radius that depends on electron energy.

1. Introduction

Active studies of plasma wakefield acceleration initiated by Tajima and Dawson (1979) for laser drivers and Chen et al. (1985) for electron drivers have reached a point where quality of accelerated beams comes to the fore. Various injection techniques are now under investigation in search of reliable ways of producing low-emittance and low-energy spread electron beams, as reviewed by Esarey et al. (2009). One promising technique is side injection of a low-energy electron bunch to the wakefield at some small angle. This method was first proposed by Kalmykov et al. (2006) to increase trapping efficiency by taking advantage of a specific wave nonlinearity. Later, injection at an angle was theoretically studied by Luttikhof et al. (2007, 2009) as a cure for ponderomotive scattering and deleterious effects on the vacuum–plasma transition. Recently, side injection has found application in proton-driven wakefield acceleration (Pukhov et al. 2011) as the means to save electrons from scattering at early stages of driver evolution in the plasma.

This study is motivated by unexpectedly good quality of the electron bunch injected from the side into the wakefield of self-modulating proton beam. Figure 1 shows the simulated energy spectra of test electrons after 4 m of wakefield acceleration for side injection and on-axis injection. The wakefield parameters are those of the half-cut super proton synchrotron–large hadron collider (SPS–LHC) beam from Caldwell and Lotov (2011). Electron bunches of 8 MeV energy, initial radius 0.2 mm, angular spread 0.6 mrad, and uniform density distribution over the wakefield period (1.26 mm) are injected after 6 m of driver propagation and accelerated up to 10 m. The injection angle is 5 mrad. Simulations are made by LCODE code (Lotov 1998). Paper by Pukhov et al. (2011) contains a similar result produced by the H-VLPL3D code for slightly different parameters of the electron bunch. The vertical scale in Fig. 1 is the fraction of the injected charge per energy interval, so 28% of injected electrons are seen to be trapped and accelerated with the final root mean square (rms) energy spread of 2% in the case of side injection. In contrast, the on-axis injection results in a wide energy spectrum as is expected for long electron bunches sampling all values of the accelerating wakefield.

The theory of side injection is still a long way from completion. It is essentially two-dimensional. The one-dimensional Hamiltonian approach of Esarey and Pilloff (1995) helps to some extent to identify rough scalings, but quantitative results necessarily rely on simulations. In this paper we make a step toward creation of a two-dimensional trapping theory and formulate necessary conditions for side-injected electrons to penetrate into the wakefield. We assume electrons are injected at a small angle α to the direction of driver propagation and show that there is an optimum value of this angle.

We first formulate the necessary mathematical framework for particle beam-driven wakes (Sec. 2), as there is a universal field asymptotic in this case. In Sec. 3 we analyze the equation obtained and find unified laws of electron penetration into the wakefield. In Sec. 4 we generalize the formalism to laser-driven wakes.

2. Particle beam-driven wakes

We use cylindrical coordinates (r, φ, z) with the drive beam propagating along the **z**-axis. The wakefield is assumed axisymmetric and unchanged in time in the driver reference frame. This assumption is justified if electron trapping occurs at a much shorter time scale than the time of driver evolution, which is typically the case. The phase velocity of the wakefield is $V_w \approx c$, the relativistic factor is $\Gamma_w = (1 - V_w^2/c^2)^{-1/2}$, where c is the speed of light.

https://doi.org/10.1017/S0022377812000335 Published online by Cambridge University Press

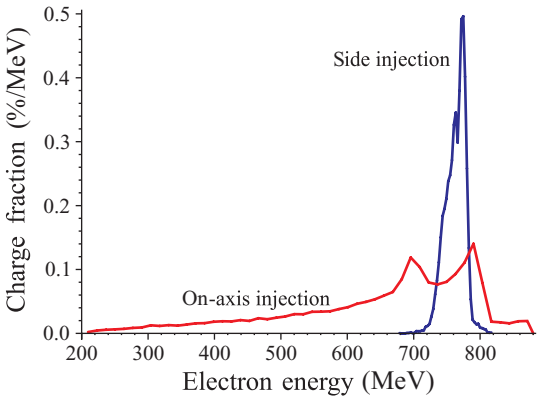


Figure 1. (Colour online) Spectra of test electrons after 4 m of proton-driven wakefield acceleration for side injection and on-axis injection.

The geometry of the problem is shown in Fig. 2. Electrons initially form a stream of velocity V directed to axis. We use the co-moving coordinate $\xi = z - V_w t$ and do not Lorentz transform the fields into the moving frame. In new coordinates, electrons move backward and radially with velocity components,

$$v_\xi = V\cos\alpha - V_w, \qquad v_r = -V\sin\alpha \approx -\alpha c. \tag{2.1}$$

As far as the side injection is usually aimed at further acceleration of electrons, we assume $V_w > V$ and $v_\xi < 0$.

Electron energies discussed in the context of side injection mostly fall in the range 3–15 MeV (Luttikhof et al. 2007, 2009; Pukhov et al. 2011), and usually the condition $\alpha \lesssim \Gamma^{-1}$ is fulfilled, where $\Gamma = (1-V^2/c^2)^{-1/2}$. As we show below, for the optimum angle the stronger condition $\alpha\Gamma \ll 1$ must be fulfilled, and we use this to neglect the angular dependence of longitudinal velocity:

$$v_\xi \approx c\left(1-\frac{1}{2\Gamma^2}\right)\left(1-\frac{\alpha^2}{2}\right) - c\left(1-\frac{1}{2\Gamma_w^2}\right)$$
$$\approx c\left(\frac{1}{2\Gamma_w^2}-\frac{1}{2\Gamma^2}\right) \approx V - V_w. \tag{2.2}$$

The force exerted on an axially moving relativistic electron is the gradient of the wakefield potential energy Φ. Side-injected electrons either fall into the potential well of the wakefield, or are reflected radially by a potential hump. The initial energy W_r of electron transverse motion is determined by the radial momentum $p_r \approx \alpha\Gamma mc$, where m is the electron mass,

$$W_r = \frac{p_r^2}{2\Gamma m} \approx \frac{\alpha^2\Gamma}{2}mc^2. \tag{2.3}$$

For small α, this energy contains the product of two small parameters (α and $\alpha\Gamma$) and is much smaller than height of any potential hump in the wakefield structures of interest. Consequently, the choice of whether electron enters the wakefield or is reflected radially is made at large radii. Once an electron is trapped by the potential well, its radial velocity quickly increases, and the electron approaches the axis with a little change in ξ-coordinate. Thus, we are interested in potential behavior at large radii where important characteristics of trapping are determined.

For the particle driver of charge density $\rho(r,\xi) = \rho_b f(r) g(\xi)$ and the linearly responding plasma, the wakefield potential energy (Chen 1987) is

$$\Phi(r,\xi) = -\frac{4\pi\rho_b e}{k_p^2}R(r)Z(\xi), \tag{2.4}$$

where

$$R(r) = k_p^2\int_0^r f(r')I_0(k_p r')K_0(k_p r)\,r'\,dr'$$
$$+k_p^2\int_r^\infty f(r')I_0(k_p r)K_0(k_p r')\,r'\,dr', \tag{2.5}$$

$$Z(\xi) = k_p\int_\xi^\infty g(\xi')\sin[k_p(\xi'-\xi)]\,d\xi', \tag{2.6}$$

$$k_p = \frac{\omega_p}{c}, \qquad \omega_p = \sqrt{\frac{4\pi n_0 e^2}{m}},$$

n_0 is the plasma density, $e > 0$ is the elementary charge, and I_0 and K_0 are zeroth order modified Bessel functions. At large radii and behind the driver, formulae (2.4)–(2.6) take the universal form,

$$\Phi(r,\xi) = \Phi_0\cos(k_p\xi + \phi_0)K_0(k_p r) \tag{2.7}$$

with the amplitude Φ_0 and phase ϕ_0 determined by the individual driver shape. Setting $\phi_0 = 0$ by the choice of origin and using the asymptotic form of Bessel function K_0, we simplify the potential energy to

$$\Phi(r,\xi) \approx \Phi_0\cos(k_p\xi)\sqrt{\frac{\pi}{2}}\frac{e^{-k_p r}}{\sqrt{k_p r}}. \tag{2.8}$$

Separation of incident electrons into trapped and reflected fractions occurs at some radius $r_0 \gg k_p^{-1}$, which we define later. Denote $\Phi_1 = \Phi(r_0, 0)$. Then in the vicinity of r_0, we can write

$$\Phi(r,\xi) \approx \Phi_1\cos(k_p\xi)\,e^{-k_p(r-r_0)}. \tag{2.9}$$

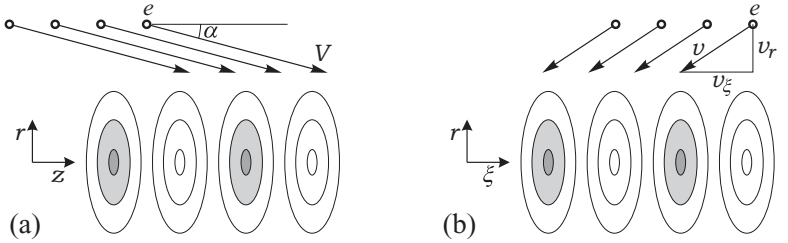


Figure 2. The geometry of the problem in (a) laboratory coordinates, and (b) co-moving coordinates.

https://doi.org/10.1017/S0022377812000335 Published online by Cambridge University Press

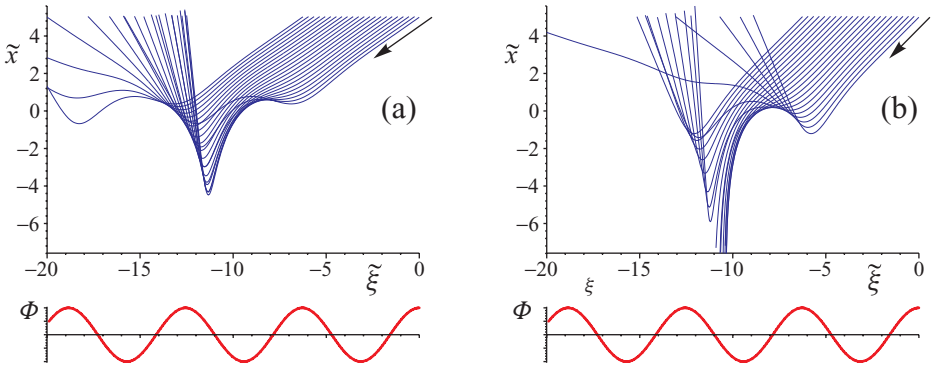


Figure 3. (Colour online) Family of electron trajectories for (a) $\tilde{v} = -0.7$, and (b) $\tilde{v} = -1$. Lower graphs show the location of potential wells and humps.

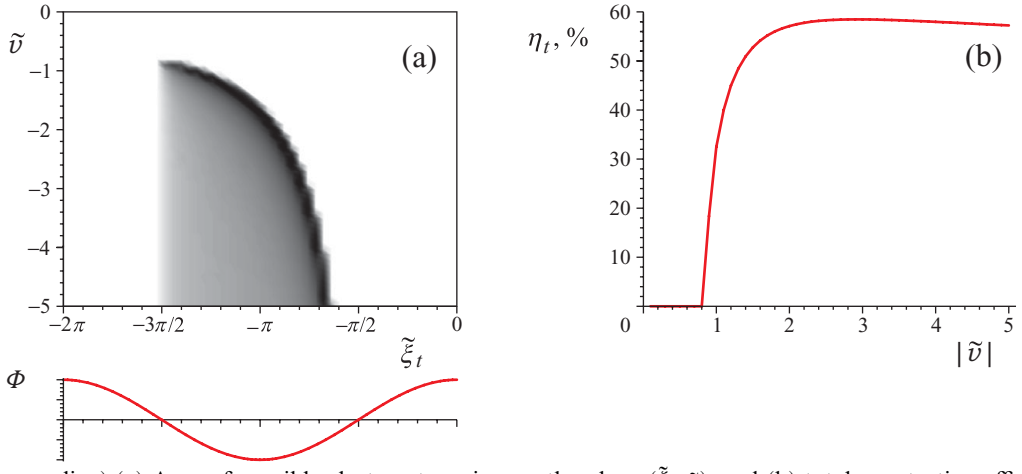


Figure 4. (Colour online) (a) Area of possible electron trapping on the plane $(\tilde{\xi}_t, \tilde{v})$, and (b) total penetration efficiency η_t as the function of the initial velocity $\tilde{v}$. The lower graph shows the location of potential wells and humps.

Equations of electron motion in the potential (2.9) are

$$\frac{dp_r}{dt} = -\frac{\partial \Phi}{\partial r} = k_p \Phi_1 \cos(k_p \xi)\, e^{-k_p(r-r_0)}, \tag{2.10}$$

$$\frac{dr}{dt} = \frac{p_r}{\Gamma m}, \qquad \frac{d\xi}{dt} = v_\xi. \tag{2.11}$$

Here we neglect the change of total electron energy, since it happens on much longer time scales. Equations (2.10)–(2.11) can be combined into one:

$$\frac{d^2 r}{dt^2} = \frac{k_p \Phi_1}{\Gamma m} \cos[k_p(v_\xi t + \xi_0)]\, e^{-k_p(r-r_0)}. \tag{2.12}$$

Introducing dimensionless variables,

$$\tilde{t} = -k_p v_\xi t, \qquad \tilde{\xi}_0 = k_p \xi_0, \qquad \tilde{\xi} = \tilde{\xi}_0 - \tilde{t},$$

$$\tilde{x} = k_p(r - r_0) - \ln\left(\frac{\Phi_1}{\Gamma m v_\xi^2}\right), \tag{2.13}$$

we rewrite (2.12) in the universal form:

$$\frac{d^2 \tilde{x}}{d\tilde{t}^2} = \cos(\tilde{t} - \tilde{\xi}_0)\, e^{-\tilde{x}}. \tag{2.14}$$

This equation must be solved with initial conditions corresponding to electron arrival from large $\tilde{x}$ with negative dimensionless velocity,

$$\tilde{v} = \frac{d\tilde{x}}{d\tilde{t}} = -\frac{v_r}{v_\xi} = \frac{\alpha c}{V - V_w}. \tag{2.15}$$

3. Penetration of electrons into the wakefield

Equation (2.14) can be easily solved numerically for any values of initial velocity $\tilde{v}$ and phase $\tilde{\xi}_0$. For low initial velocities, all electrons are reflected by the outer region of the wakefield (Fig. 3(a)). For larger $\tilde{v}$, there are two types of electron trajectories (Fig. 3(b)). Depending on the phase, electrons either penetrate the wakefield, or are reflected. The electrons that entered into the wakefield are quickly accelerated radially and stick to some phase $\tilde{\xi}_t$. This is exactly the phase of the wakefield into which the injection of electrons occurs.

General picture of electron penetration is shown in Fig. 4(a). Electrons cannot enter the wakefield at phases and initial velocities marked by the white color. The darker the color, the greater the flux density F_t of entered electrons, i.e. the number of electrons trapped in the unit interval of $\tilde{\xi}_t$ divided by the number of incoming electrons passing through the unit interval of $\tilde{\xi}$ at large radii. The total penetration efficiency η_t (into all

https://doi.org/10.1017/S0022377812000335 Published online by Cambridge University Press

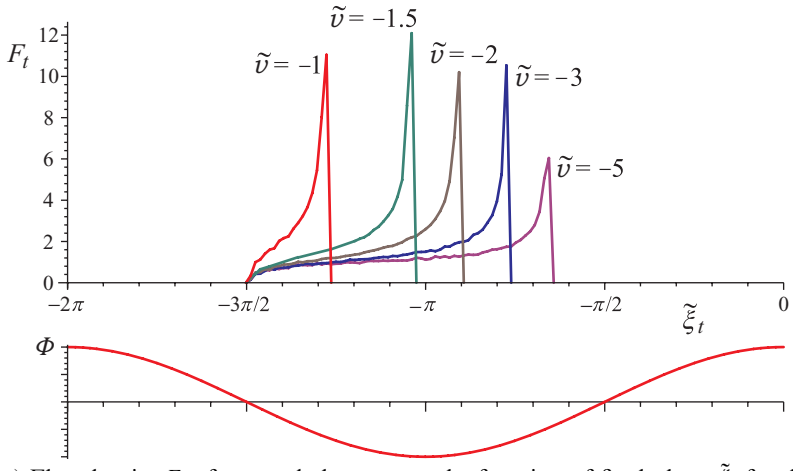


Figure 5. (Colour online) Flux density F_t of trapped electrons as the function of final phase $\tilde{\xi}_t$ for different values of initial velocity $\tilde{v}$. Thin line is the flux density of incoming electrons. The lower graph shows the location of potential wells and humps.

phases) is shown in Fig. 4(b). The penetration threshold is observed at $\tilde{v} \approx -0.81$. For $|\tilde{v}| \gtrsim 1$, not only more than half of the electrons penetrate into the wakefield but the electron flux density also increases several times (Fig. 5). In other words, injection of electrons preferably occurs into a certain phase of the wakefield, and this phase depends on the dimensionless radial electron velocity $\tilde{v}$.

Penetration of an electron into the wakefield does not mean this electron is trapped by the wakefield. The initial radial velocity of the electron can be too high, or the energy gained by the electron in near-axis regions can be insufficient for trapping. In these cases, the electron crosses the axis and leaves the wakefield on the opposite side. The lower the initial radial velocity of the electron, the easier the electron to be trapped. Consequently, there is an optimum angle of electron injection corresponding to $|\tilde{v}| \sim 1$. It is just above the penetration threshold:

$$\alpha_{\mathrm{opt}} \sim \frac{V_w - V}{c}. \tag{3.1}$$

If the relativistic factor of the wave is much greater than that of the electron, $\Gamma_w \gg \Gamma$, we obtain the following engineering formula:

$$\alpha_{\mathrm{opt}} \sim \frac{1}{2\Gamma_w^2}. \tag{3.2}$$

For $\Gamma_w \sim \Gamma$, the optimum angle is even smaller. Estimate (3.2) justifies the condition $\alpha\Gamma \ll 1$ and formula (2.2).

As we see from Fig. 3, separation of incident electrons occurs at $\tilde{x} \approx 0$. Let us find the corresponding dimensional radius r_0. Substituting $\tilde{x} = 0$ and $r = r_0$ into the definition of $\tilde{x}$ (2.13), we find

$$\Phi(r_0, 0) = \Gamma m v_\xi^2. \tag{3.3}$$

Using approximation (2.8) for Φ_1, assuming $\Gamma_w \gg \Gamma$, and limiting ourselves to the logarithmic accuracy, we obtain a quick estimate for the reflection radius:

$$r_0 \approx k_p^{-1} \ln\left(\frac{\Phi_0 \Gamma^3}{mc^2}\right). \tag{3.4}$$

4. Laser beam-driven wakes

For laser drivers, there is no universal asymptotic form of wakefield potential at large radii. The wakefield potential energy is determined by the vector potential of driver $\mathbf{A}$ (Esarey et al. 2009):

$$\Phi(r, \xi) = -mc^2 k_p \int_\xi^\infty \frac{\mathbf{a}^2(r, \xi')}{2} \sin[k_p(\xi' - \xi)]\, d\xi', \tag{4.1}$$

$$\mathbf{a} = \frac{e\mathbf{A}}{mc^2}.$$

Usually $\Phi(r, \xi)$ follows the same radial dependence as $\mathbf{A}^2(r, \xi)$ does. This dependence does not necessarily have an exponential asymptotic at large radii. Nevertheless, the results of Sec. 3 are still applicable to laser-driven fields, though with a lower accuracy. We can approximate the potential energy in the vicinity of separation radius r_0 by the proper exponent function:

$$\Phi(r, \xi) \approx \Phi_1 \cos(k_p \xi)\, e^{-\lambda(r - r_0)}. \tag{4.2}$$

For example, for a Gaussian driver of the radius σ_r we have

$$\mathbf{a}^2 \propto e^{-r^2/\sigma_r^2}, \quad \Phi(r_0 + \delta r, \xi) = \Phi_1 \cos(k_p \xi)\, e^{-2r_0 \delta r/\sigma_r^2 - \delta r^2/\sigma_r^2},$$
$$\lambda = 2r_0/\sigma_r^2. \tag{4.3}$$

As far as $\lambda \neq k_p$, (2.12), definition of $\tilde{x}$ (2.13), and the initial velocity (2.15) need to be modified:

$$\frac{d^2 r}{dt^2} = \frac{\lambda \Phi_1}{\Gamma m} \cos[k_p(v_\xi t + \xi_0)]\, e^{-\lambda(r - r_0)}. \tag{4.4}$$

$$\tilde{x} = \lambda(r - r_0) - \ln\left(\frac{\Phi_1 \lambda^2}{\Gamma m v_\xi^2 k_p^2}\right), \quad \tilde{v} = \frac{d\tilde{x}}{d\tilde{t}} = -\frac{v_r \lambda}{v_\xi k_p}. \tag{4.5}$$

In newly defined variables, (2.14) remains unchanged, as are the results of Sec. 3 presented in Figs. 3–5. We need to modify only expression (3.1) for α_{opt} and expression

https://doi.org/10.1017/S0022377812000335 Published online by Cambridge University Press

(3.3) for r_0:

$$\alpha_{\mathrm{opt}} \sim \frac{(V_w - V)k_p}{c\lambda}, \tag{4.6}$$

$$\Phi(r_0,0)\lambda^2(r_0) = \frac{1}{\Phi(r_0,0)}\left(\frac{\partial\Phi(r_0,0)}{\partial r_0}\right)^2 = \Gamma\, m v_\xi^2 k_p^2. \tag{4.7}$$

5. Summary

Let us summarize the main findings. There is an optimum angle for side injection of electrons into the plasma wakefield as is given by formula (3.1) or (4.6). At smaller angles, all electrons are reflected back. At larger angles, electrons enter the wakefield with superfluous transverse momentum that is unfavorable for trapping.

Penetration efficiency and the wakefield phase into which electrons enter are determined by the field behavior at large radii. In most cases, the wakefield there decays exponentially, and the process of electron entrance into the wakefield can be studied in a unified way.

Although formulated for linear wakefields, the results of the paper are also applicable to nonlinear wakes if the latter have a factorable field asymptotic of the form (4.2).

Acknowledgements

This work is supported by the Ministry of Education and Science of the Russian Federation, RFBR (Grants 11-01-00249 and 11-02-00563), Grant 11.G34.31.0033 of the Russian Federation Government, and RF President's Grant NSh-5118.2012.2.

References

Caldwell, A. and Lotov, K. V. 2011 Plasma wakefield acceleration with a modulated proton bunch. *Phys. Plasmas* **18**, 103101.

Chen, P. 1987 A possible final focusing mechanism for linear colliders. *Part. Accel.* **20**, 171–182.

Chen, P., Dawson, J. M., Huff, R. W. and Katsouleas, T. 1985 Acceleration of electrons by the interaction of a bunched electron beam with a plasma. *Phys. Rev. Lett.* **54**, 693–708.

Esarey, E. and Pilloff, M. 1995 Trapping and acceleration in nonlinear plasma waves. *Phys. Plasmas* **2**, 1432–1436.

Esarey, E., Schroeder, C. B. and Leemans, W. P. 2009 Physics of laser-driven plasma-based electron accelerators. *Rev. Mod. Phys.* **81**, 1229–1285.

Kalmykov, S. Y., Gorbunov, L. M., Mora, P. and Shvets, G. 2006 Injection, trapping, and acceleration of electrons in a three-dimensional nonlinear laser wakefield. *Phys. Plasmas* **13**, 113102.

Lotov, K. V. 1998 Simulation of ultrarelativistic beam dynamics in plasma wake-field accelerator. *Phys. Plasmas* **5**, 785–791.

Luttikhof, M. J. H., Khachatryan, A. G., van Goor, F. A. and Boller, K. J. 2007 The effect of the vacuum–plasma transition and an injection angle on electron-bunch injection into a laser wakefield. *Phys. Plasmas* **14**, 083101.

Luttikhof, M. J. H., Khachatryan, A. G., van Goor, F. A., Boller, K. J. and Mora, P. 2009 Electron bunch injection at an angle into a laser wakefield. *Laser Part. Beams* **27**, 69–77.

Pukhov, A., Kumar, N., Tuckmantel, T., Upadhyay, A., Lotov, K., Muggli, P., Khudik, V., Siemon, C.and Shvets, G. 2011 Phase velocity and particle injection in a self-modulated proton-driven plasma wakefield accelerator. *Phys. Rev. Lett.* **107**, 145003.

Tajima, T. and Dawson, J. M. 1979 Laser electron accelerator. *Phys. Rev. Lett.* **43**, 267–270.

https://doi.org/10.1017/S0022377812000335 Published online by Cambridge University Press